Application of a differentiator-based adaptive super-twisting controller for a redundant cable-driven parallel robot

Application of a Differentiator-Based Adaptive Super-Twisting Controller for a Redundant Cable-Driven Parallel Robot

Christian Schenk and Carlo Masone and Andreas Pott and Heinrich H. Bülthoff

Abstract In this paper we present preliminary, experimental results of an Adaptive Super-Twisting Sliding-Mode Controller with time-varying gains for redundant Cable-Driven Parallel Robots. The sliding-mode controller is paired with a feed-forward action based on dynamics inversion. An exact sliding-mode differentiator is implemented to retrieve the velocity of the end-effector using only encoder measurements with the properties of finite-time convergence, robustness against perturbations and noise filtering. The platform used to validate the controller is a robot with eight cables and six degrees of freedom powered by 940 W compact servo drives. The proposed experiment demonstrates the performance of the controller, finite-time convergence and robustness in tracking a trajectory while subject to external disturbances up to approximately 400% the mass of the end-effector.

1 Introduction

Cable-Driven Parallel Robots (*CDPR*) are systems that use elastic cables to guide the so called end-effector through space. Each cable is connected on one side at the end-effector and guided by several pulleys to ground mounted motors on the other side. These motors coil and uncoil the cables, apply a wrench at the platform and by doing this, change the position and orientation of the end-effector. Compared to other manipulators such as Steward Platforms or serial manipulators, CDPR have some outstanding advantages such as large workspace, modularity, mobility and scalability. Furthermore, because of their parallel structure and light-weight construction, CDPR have the ability to exert high accelerations. Thanks to these properties, the potential applications of CDPR are numerous and diverse and include pick and place tasks [4], rehabilitation [21], entertainment [2], simulation of motion [12] and telescopes [3]. Regardless of the application, it is of paramount importance to ensure stability and adequate performance (according to some suitable metric) in spite of possible unmodelled effects, external disturbances (e.g. wind gusts for a radio telescope) and uncertain or varying parameters (e.g. varying mass in pick and place tasks).

Christian Schenk, Carlo Masone and Heinrich H. Bülthoff
Max Planck Institute for Biological Cybernetics, Spemannstraße 38, 72076 Tübingen, Germany, contact e-mail: christian.schenk@tuebingen.mpg.de

Andreas Pott
ISW Univ. Stuttgart, 70174 Stuttgart, Germany, e-mail: andreas.pott@isw.uni-stuttgart.de

Several strategies have been proposed in the literature of CDPR to deal with perturbations, and they are often based on the adaptation of kinematic/dynamic parameters ([1, 4, 6]). However, this approach only considers parametric uncertainties and assumes the knowledge of an upper bound of the perturbations to choose the control gains. Unfortunately, in practice such an upper bound is typically unknown and one must resort to overly conservative estimates of the perturbations, which means unnecessarily high control actions and noise amplification. Another approach to deal with perturbations is to use control laws that are implicitly robust, such as sliding mode controllers [4], yet the problem of tuning the gains according to a worst case scenario persists. Additionally, sliding-mode controllers suffer from chattering effects [19] which can reduce the performance of the system and even damage its components. To overcome these limitations we proposed a robust sliding-mode controller with adaptive gains (*ASTC*) [16], based on [20], that does not require the knowledge of an upper bound of the perturbations. In [16] the controller was successfully validated in a numerical simulation, demonstrating the capability of tracking desired trajectories in operational space (i.e. pose of the end-effector) in presence of parameter uncertainties and external disturbances. Moreover, the positive effect of the adaptive control gains was remarked by a comparison with a continuous sliding mode controller with fixed gains [4] showing that, for comparable tracking error, the adaptive strategy in the ASTC effectively reduces chattering.

In this paper we present the first tests of the ASTC with a real CDPR. Our goal is to assess whether the performance of the ASTC that was obtained in simulation still holds in practice and, if not, to get a better understanding of the limiting factors. Indeed, the results of this paper show that the resilience of the controller to perturbations and the property of finite time convergence are preserved but with worse performance in terms of tracking error. In comparison to [16], another novelty of this paper is the introduction of an adaptive sliding mode differentiator [19] to indirectly derive the velocity of the end-effector using only encoders at the winches and the Forward Kinematics (*FK*) model [13,18], that is the barest minimum sensor information usually available in CDPR. The results demonstrate also the robustness and finite time convergence of the differentiator.

This paper is structured as follows: in Sec. 2 we present the model, in Sec. 3 we discuss the control strategy as well as a robust sliding-mode differentiator. Section 4 describes the experimental setup and the evaluation of the results.

2 Modeling

The control algorithm and the kinematic relations of the system considered in this paper are based on a simplified model of a redundant CDPR with $n = 6$ degrees of freedom (*dof*) and $m = 8$ massless and inextensible cables. The choice of neglecting the dynamics of the cables is an obvious abstraction of reality that is quite common in literature since this is an open topic of research. Additionally, we assume that each cable leaves the corresponding winch from a fixed point, i.e. the rotation of the winches is considered negligible. With this simplifications the generic *i*-th cable forms a straight line[17] that connects a point B_i on the end-effector (*onboard connection*) to the fixed point A_i (*offboard connection*) on the winch (Fig. 1). For the derivation of the main kinematic and dynamic relations of the system we define two frames of reference: a frame $\mathscr{F}_E = \{\mathscr{O}_E, \mathbf{X}_E, \mathbf{Y}_E, \mathbf{Z}_E\}$, fixed on the geometrical center of the end-effector and an inertial world frame $\mathscr{F}_W = \{\mathscr{O}_W, \mathbf{X}_W, \mathbf{Y}_W, \mathbf{Z}_W\}$. With this setting the pose of the end-effector w.r.t $\mathscr{F}_W$ will be denoted by

the vector $x_\nu = [p^T \nu^T]^T \in SE(3)$ where $p = [x\,y\,z]^T \in \mathbb{R}^3$ is the position and $\nu = [\phi\,\theta\,\psi]^T \in SO(3)$ is the orientation expressed as Euler angles[1].

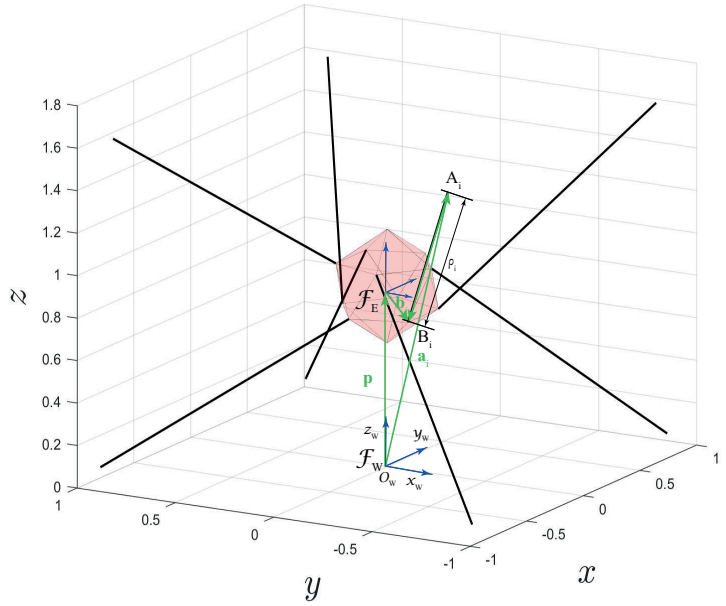

Fig. 1: Sketch of the cable robot.

2.1 Kinematics

The kinematics of CDPR describe the relation between the pose x_ν of the end-effector and the vector $\rho = [\rho_1, \rho_2, \ldots, \rho_n]^T \in \mathbb{R}^{n\times 1}$ of lengths of the cables. In particular the forward kinematics (FK) describes the mapping from ρ to x_ν, whereas the inverse kinematics (IK) describes the inverse mapping. Both the IK and FK are relevant for the implementation of the controller and are briefly discussed in the following.

Inverse Kinematics

Thanks to the simplifying assumptions made so far, the IK of a fully constrained CDPR has a closed form solution. Formally, the mapping from x_ν to the length ρ_i of each cable i can be written in the form of a polygonal constraint (see Fig. 1), i.e.

[1] In the experiments we use the ZYX (roll-pitch-yaw) sequence.

$$\|^W l_i\| = \|\rho_i {}^W n_i\| = \rho_i = \|^W a_i - p - {}^W R_E {}^E b_i\|, \tag{1}$$

where ${}^W n_i$ is the support unit vector of the cable, $a_i \in \mathbb{R}^3$ is the position vector of A_i w.r.t. $\mathscr{F}_{\mathscr{W}}$, ${}^W R_E {}^E b_i = {}^W b_i \in \mathbb{R}^3$ is the vector $\overrightarrow{O_E B_i}$ expressed in $\mathscr{F}_{\mathscr{W}}$ and ${}^W R_E$ is the rotation matrix that expresses the orientation of $\mathscr{F}_{\mathscr{E}}$ w.r.t. $\mathscr{F}_{\mathscr{W}}$. Differentiating (1) with respect to time leads to the well-known differential equation

$$\dot{\rho} = \underbrace{\begin{bmatrix} -{}^W n_1^T & -({}^W R_E {}^E b_i \times {}^W n_i)^T \\ \vdots & \vdots \\ -{}^W n_n^T & -({}^W R_E {}^E b_n \times {}^W n_n)^T \end{bmatrix}}_{J} \dot{x}. \tag{2}$$

with the vector $\dot{x} = [p^T, {}^W \omega^T]^T$ describing the velocity of the rigid body end-effector by using angular velocities[2] and the Jacobian matrix J. It will be shown in Sec. 2.2 that the Jacobian J also plays a role in mapping forces exerted by the cables (cable tension) to wrenches applied to the end-effector.

Forward Kinematics

When considering the problem of tracking a trajectory of the end-effector using only the measurements given by the encoders at the winches (i.e. measurements of the lengths of the cables) we need to solve the FK problem to indirectly retrieve the current pose of the end-effector. Since the FK for a fully constrained CDPR in general does not have a unique solution [7] we address it as an optimization problem, i.e.

$$x_{FF}^\star = \min_{p^\star, v^\star} \Psi_{FF}(l, p, v) = \min_{p^\star, v^\star} \sum_{i=1}^{n} \{(\rho_i - \hat{\rho}_i(p, v))\} \tag{3}$$

in which the cost function $\Psi_{FF}(l, p, v)$ is the error between the measured cable lengths and the cable lengths from the kinematic relation (1), and $(\bullet)^\star$ denotes the optimal solution. It has been shown in [8–10] that problem 3 can be solved efficiently by using the method from levenberg-marquardt (*lm*), an iterative algorithm that updates the solution of the optimization problem with the following rule

$$x_{lm,k+1} = x_{lm,k} + h_{lm,k}, \tag{4}$$

where $h_{lm,k}$ is the update computed at the step k. The update step $h_{lm,k}$ in (4) is determined by solving the equation

$$\left(J(x_{lm,k})^T J(x_{lm,k}) + \lambda_{lm} I_n\right) h_{lm,k} = J(x_{lm,k})^T (\rho - \hat{\rho}(x_k)). \tag{5}$$

Note that in (5) the term λ_{lm} is a damping factor that modifies the singular values of the matrix $\left(J(x_{lm,k})^T J(x_{lm,k}) + I_n\right)$ to make it better conditioned close to singularities of J. The algorithm stops when the update step becomes small enough, i.e. when $\|x_{lm,k+1} - x_{lm,k}\| < \varepsilon_{lm}$ with a predefined threshold $\varepsilon_{lm} \in \mathbb{R}$. In practice we found that an acceptable solution would be usually found in less than 20 iterations by using the previous solution as initial guess for the optimization [14].

[2] Note that $\dot{x} \neq \frac{d}{dt} x_v$ since ${}^W \omega \neq \dot{v}$

2.2 Dynamics

The dynamics of the CDPR provide a relation between the tensions of the cables and their effect onto the motion of the end-effector. Given a nominal mass $m \in \mathbb{R}$, a nominal inertia $I_E \in \mathbb{R}^{3\times3}$ w.r.t. $\mathscr{F}_E$ and the position of the center of mass ${}^W c = [c_x, c_y, c_z]^T$ in $\mathscr{F}_W$ and using either the Newton-Euler or Euler-Lagrange approach, the dynamics of the system are expressed by a second order ordinary differential equation

$$B(x_v)\ddot{x} + C(x_v, \dot{x})\dot{x} - g(x_v) = u = -J^T t \tag{6}$$

$$B(x_v) = \begin{bmatrix} mI_3 & m\,{}^W c\times^T \\ m\,{}^W c\times & H \end{bmatrix}, \tag{7}$$

$$C(x_v, \dot{x})\dot{x} = \begin{bmatrix} m\,{}^W\omega\times\,{}^W\omega\times\,{}^W c \\ {}^W\omega\times H\,{}^W\omega \end{bmatrix}, \tag{8}$$

$$g(x_v) = \begin{bmatrix} 0 & 0 & -mg & -mc_y g & mc_x g & 0 \end{bmatrix}^T \tag{9}$$

$$H = {}^W R_E\,{}^E I_E\,{}^E R_W + m\,{}^W c\times\,{}^W c\times^T. \tag{10}$$

where $t \in \mathbb{R}^{8\times1}$ is the vector of cable tensions, $u \in \mathbb{R}^{6\times1}$ is the wrench applied to the end-effector and $(\bullet)\times$ is the well-known cross-product operator.

To formulate the control we need to rewrite the model (6) to (10) in regular form. For this purpose, let us first denote the full state of the system as the 12×1 vector $\bar{x} = [x_v^T\ \dot{x}^T]^T = [p^T\ v^T\ \dot{p}^T\ {}^W\omega^T]^T$ and the output as $x_v = [p^T\ v^T]$. Now we define the diffeomorphism Ω that brings the system in regular form as

$$z = \begin{bmatrix} z_1 \\ z_2 \end{bmatrix} = \Omega(\bar{x}) = \begin{bmatrix} I_6 & 0_{6\times6} \\ 0_{6\times6} & \underbrace{\begin{bmatrix} I_3 & 0_{3\times3} \\ 0_{3\times3} & {}^v E_\omega \end{bmatrix}}_{A(x_v)} \end{bmatrix} \bar{x}. \tag{11}$$

Finally, applying (11) and using the new state vector $\bar{x}$ on (6) we obtain the regular form

$$\begin{cases} \dot{z}_1 = z_2 \\ \dot{z}_2 = f(\bar{x}) + h(\bar{x})u \end{cases} \tag{12}$$

with

$$\begin{aligned} f(\bar{x}) &= -A(x_v)B^{-1}(x_v)\left[C(x_v, \dot{x})\dot{x} - g(x_v)\right] \\ &\quad + \dot{A}(x_v, \dot{x})\dot{x} \end{aligned} \tag{13}$$

$$h(\bar{x}) = A(x_v)B^{-1}(x_v) \tag{14}$$

Remark 1. *To ensure that ${}^v E_\omega$ is not singular and $h(\tilde{x})$ has rank m, we limit the pitch angle θ to $\left(-\frac{\pi}{2}, \frac{\pi}{2}\right)$.*

As mentioned earlier, this model is a simplified representation of reality and it may contain unmodelled effects such as slip-stick effects, breakaway torque, etc.. The model (12) can be extended to incorporate model uncertainties and external wrench disturbances ζ as follows

$$\begin{cases} \dot{z}_1 & = z_2 \\ \dot{z}_2 & = f_n(\bar{x}) + \Delta f(\bar{x}) + h_n(\bar{x}) \cdot \big(u + \zeta\big) + \Delta h(\bar{x}) \cdot \big(u + \zeta\big) \\ & = f_n(\bar{x}) + h_n(\bar{x}) u + \xi \end{cases} \tag{15}$$

where

- f_n and h_n indicate the nominal model of the robot;
- $\Delta(\bullet)$ contains the unmodelled effects and parameter uncertainties;
- $\xi = h_n(\bar{x})\,\zeta + \Delta f(\bar{x}) + \Delta h(\bar{x}) \cdot (u + \zeta)$ is the vector of lumped perturbations.

As mentioned in Sec. 1, in nominal working conditions the lumped perturbations of a physical system reasonably have an upper bound but this upper bound is not known. Thus, we make the following assumption

Assumption 1. *ξ is bounded by an unknown upper bound ξ_{max} such that $0 \leq |\xi|_2 \leq \xi_{max}$.*

3 Control and State Differentiation

Using the model developed in Sec. 2, we can now design the control input u in (15) to let the end-effector track a desired trajectory $z_{1,d} = [p_d^T \; \nu_d^T]^T \in SE(3)$ that is provided with its derivatives $z_{2,d} = [\dot{p}_d^T \; \dot{\nu}_d^T]^T$ and $\dot{z}_{2,d} = [\ddot{p}_d^T \; \ddot{\nu}_d^T]^T$, assuming also the presence of perturbations. The solution that we propose combines a feed-forward control action u_{FF} based on the inversion of the nominal dynamic model, and a term based on a robust sliding-mode controller. The full control input then becomes:

$$u = u_{SM} + u_{FF}. \tag{16}$$

where u_{FF} is a feed-forward input and u_{SM} is the control action of the sliding-mode controller.

Before venturing in the details of the terms forming the control wrench u we must point out that not all wrenches are feasible, due to the possible presence of singularities in the Jacobian J and to the fact that the tensions t that can be exerted by the cables are limited within a non-negative range[3], i.e. $0 \leq t_{min} \leq t \leq t_{max}$. Hereinafter we will simply assume that u is within the admissible range of wrenches that defines the wrench-feasible-workspace of the robot. Nevertheless, in the next section it will be shown that the sliding-mode control u_{SM} embeds a saturation that can be tuned according to the feasible range of wrenches. Due to lack of space, we will not perform an analysis of the range of feasible wrenches for our robot, however the experiment presented in Sec. 4 will demonstrate that with suitable tuning of the controller and a reasonable desired trajectory the control wrench u is always feasible. Lastly, the cable tensions that need to be commanded by the motors to implement u can be safely obtained using one of the many tension distribution algorithms that are available in literature (e.g. [6, 11, 15]).

3.1 Control Design

ASTC: To steer the tracking error $e = z_{1,d} - z_1$ and its derivative $\dot{e} = z_{2,d} - z_2$ to zero we choose as sliding variable $\sigma = \dot{e} + \Lambda e$ where Λ is a positive definite matrix of proper size. To achieve $\sigma = \dot{\sigma} = 0$ with σ

[3] The cables can only pull the end-effector, not push it. Hence the tension in a cable can never be negative.

we implement u_{SM} as a super-twisting controller [19]. Moreover, to overcome the disadvantages of constant high chosen gains, we use the adaptation law proposed by Shtessel in [20]. The full expression of u_{SM} is given by:

$$u_{SM} = -\alpha\,|\sigma|^{\frac{1}{2}}\,\mathrm{sign}\,(\sigma) + v \tag{17}$$

$$\dot{v} = \begin{cases} -u_{SM} & \text{if } |u_{SM}| > \overline{u} \\ -\beta\,\mathrm{sign}\,(\sigma) & \text{if } |u_{SM}| \leq \overline{u} \end{cases} \tag{18}$$

$$\dot{\alpha} = \begin{cases} \omega_\alpha \sqrt{\dfrac{\gamma}{2}}\,\mathrm{sign}\,(|\sigma| - \mu), & \text{if } \alpha > \alpha_m \\ \eta, & \text{if } \alpha \leq \alpha_m \end{cases} \tag{19}$$

$$\beta = 2\,\varepsilon\,\alpha \tag{20}$$

$$\mu(t) = 4\,\alpha(t)\,T_e\,, \tag{21}$$

where

- $\overline{u}$,$\underline{u}$ are the upper and lower bound for u_{SM};
- α, β are positive definite diagonal matrices of gains;
- $\omega_\alpha, \gamma, \eta, \alpha_m$ are positive constants that determine the update rate of the gains (we refer the reader to [20] for more details;
- T_e is the sampling period for the controller.

Feedforward: One important characteristic of the ASTC is that the input u_{SM} is continuous, since the discontinuity in (18) is passed through an integrator. While this helps to reduce numerical chattering, this effect is not completely removed. The feedforward input u_{FF} in (16) is meant to reduce the control effort of the ASTC and thus also reduce chattering and noise amplification. The term u_{FF} is based on dynamic inversion of the nominal model, using the reference trajectory $x_v d$, $\dot{x}_d$ and $\ddot{x}_d$. Formally, inverting the dynamics presented in Sec. 2.2 yields

$$u_{FF} = u = B(x_{v,d})\ddot{x}_d + C(x_{v,d}, \dot{x}_d)\dot{x}_d - g(x_{v,d}) \tag{22}$$

3.2 Sliding-Mode Differentiator

In order to implement the control input u_{SM} we need to measure both z_1 and z_2 or, equivalently, the pose x_v and velocity $\dot{x}$ of the end-effector and use (11). For the the pose x_v, as explained in Sec. 2.1, we can retrieve it from the encoders measurements by solving the FK problem. However, to obtain the velocity $\dot{x}$ from the positional encoders we must resort to a numerical differentiator. Hence, using the same principles of the ASTC, we implemented a first order sliding mode differentiator [19]. The advantage of this family of differentiators is that it achieves finite time convergence and exact stabilization, besides having the robustness properties of a sliding mode algorithm. For detailed information on sliding mode differentiators and their properties we refer the reader to [19]. Here we just show the final equation of the differentiator, i.e.

$$\begin{aligned} \dot{\tilde{x}}_0 &= -\lambda_1 L^{\frac{1}{4}}\,\|\tilde{x}_0 - x\|^{\frac{1}{2}}\,\mathrm{sign}\,(\tilde{x}_0 - x) + \tilde{x}_1 \\ \dot{\tilde{x}}_1 &= -\lambda_0 L\,\mathrm{sign}\,(\tilde{x}_0 - x) \end{aligned} \tag{23}$$

where

- $\tilde{x}_0$ and $\tilde{x}_0$ are the estimates of x_v and $\dot{x}_v$, respectively[4].
- λ_1 and λ_2 are the gains of the differentiator. As suggested in [19], we tuned these gains as $\lambda_1 = 1.1$ and $\lambda_2 = 1.3$.
- L is the Liepschitz constant of the last derivative estimated by the differentiator, in this case $\dot{x}_v$. In practice this value determines the cutoff frequency of the differentiator. We used the value $L = 15$.

4 Experimental Validation

The robot used to validate the proposed control algorithm is a redundant CDPR with 6 dof that was custom built at the Max Planck Institute for Biological Cybernetics (see Fig. 2). The end-effector of the robot is an icosahedron platform made of aluminium. The nominal mass of the end-effector is $m = 2.6$ kg and its nominal inertia tensor with respect to the principal axes is ${}^E I_E = diag\{[0.04613, 0.04613, 0.04873]\}$ Nm^2. The system is powered by eight 940 W compact servo drives of type Beckhoff AM8033-0E21 with a drum diameter of 39.15 mm, that are located under the metal base of the frame. These actuators allow to exert a maximum cable force of 878 N.

On the software side, we used an off-the-shelves Beckhoff TwinCAT software (*Windows Control and Automation Technology*) to control the robot and interface with the sensors. TwinCAT offers the possibility to run simultaneously multiple Programmable Logic Controllers (*PLC*) in real-time and it provides both a runtime environment for real time NC-axis control and a programming environment for code development. Moreover, this software allows to implement the low-level control of the drives both giving a target cable length (position control) or a target torque (torque control). In our experiment we used this second mode of operation because the control input from our ASTC algorithm is the applied wrench, i.e. the tension of the cables.

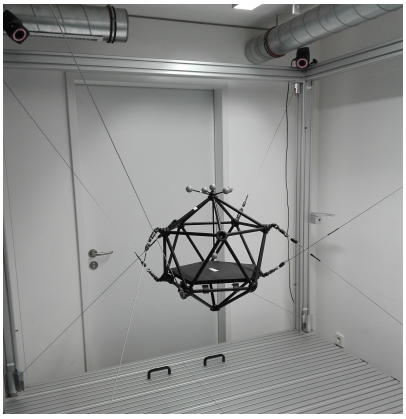

Fig. 2: Mini CableRobot Simulator.

[4] Note that the differentiator estimates $\dot{x}_v$, however the transformation from $\dot{x}_v$ to $\dot{x}$ is straightforward.

Table 1: Kinematic parameters

Kinematic parameters																
	a_1	a_2	a_3	a_4	a_5	a_6	a_7	a_8	b_1	b_2	b_3	b_4	b_5	b_6	b_7	b_8
x [m]	-0.907	-0.853	0.911	0.871	0.907	0.860	-0.900	-0.870	-0.127	-0.206	0.014	0.134	0.135	0.008	-0.143	-0.220
y [m]	0.871	0.965	0.820	0.918	-0.845	-0.928	-0.829	-0.935	0.177	0.065	0.239	0.175	-0.186	-0.241	-0.206	-0.082
z [m]	1.640	0.0675	1.590	0.079	1.610	0.079	1.600	0.063	0.115	-0.111	-0.102	0.122	-0.101	0.114	-0.092	0.107

Visible in Fig. 2 is also a set of near-infrared cameras (we have four in total) from VICON[5] with a sampling frequency of 250Hz that can be used to track the pose of the platform with a precision of 0.5mm thanks to a set of reflective markers mounted on the top of the end-effector. We want to stress that the VICON tracking system was not used in the experiments, during which we only used encoder measurements. This is due to the fact that an external vision based tracking system like the one from VICON is rarely used with large size CDPR like our CableMotion Simulator [12]. The VICON tracking system has only been used before the experiment to calibrate the kinematic parameters a_i and b_i in (1). To perform the calibration the end-effector was moved throught the operational workspace, taking care to excite as much as possible the full range of translations and rotations, meanwhile recording both the length measurements ρ from the encoders and the pose meaurement x_v from the visual tracker. With these measurements the kinematic parameters a_i and b_i for the generic i-th cable are calibrated by solving a quadratic minimization problem over all N measurement samples, i.e.

$$\begin{bmatrix} a_i^\star \\ b_i^\star \end{bmatrix} = \min_{a_i,b_i} \left\{ \sum_{j=1}^{N} \rho_{i,j} - \| {}^W a_i - p - {}^W R_E {}^E b_i \|^2 \right\} \quad \text{s.t. } a_i \in [\underline{a}, \overline{a}],\ b_i \in [\underline{b}, \overline{b}] \tag{24}$$

where $\underline{a}$, $\overline{a}$ and $\underline{b}$, $\overline{b}$ are the boundaries of the search region. The results are reported in Tab. 1.

4.1 Results

To validate the proposed ASTC algorithm we performed an experiment in which the end-effector is tasked to follow the predefined trajectory $p_d = [0.15+0.15cos(\omega \cdot t - \frac{\pi}{2}), -0.145+0.15+0.15sin(\omega \cdot t - \frac{\pi}{2}), 0.85]$ m, $\nu_d = [0,0,0]^\circ$ with $\omega = 0.5$. The parameters of the control algorithm (17) to (19) and (21) were set to $\varepsilon = 0.3$, $\gamma = 1$, $\omega_\alpha = 21.213$.

In order to use the ASTC control law we first need to retrieve the measurement of the state of the system, i.e. the pose x_v and velocity $\dot{x}$ of the end-effector. Recalling our previous discussion, the pose can be reconstructed from the encoder measurements ρ by solving the FK problem whereas the velocity, not being directly available, is obtained from the Sliding-Mode Differentiator (*SMD*) (23). The finite-time convergence of the differentiator is confirmed byFigs. 3a and 3b where it is visible that the pose from the SMD rapidly converges to the pose from the FK. For the velocity, lacking a measurement of $\dot{x}$ to compare the output of the SMD with, we computed the numerical derivative of the encoder measurement ρ and then used the differential kinematics (2) to get $\dot{x}$. Using this as a comparison, Figs. 3c and 3d show that, for our choice of parameters in Sec. 3.2, the velocity estimate from the SMD follows the mean of the numerical derivative but filters noise.

[5] http://vicon.com/

Having assessed the correct operation of the SMD we can now look at the performance of the ASTC, its robustness in particular. In this regard, the controller has to face three different kinds of perturbations. Firstly, parameter uncertainties, because the nominal physical parameters of the end-effector have been derived from an approximated CAD model and therefore it is reasonable to expect deviations from the real values. Secondly, unmodelled dynamics, since in our model we considered an extremely simplified power-train with ideal cables and without transients or other effects in the drives. Lastly, external disturbances, because to make the task more challenging we applied external wrenches to the platform while it was moving. More specifically:

1. From 55s to 61s a 5 kg disk ($\approx 192\%$ the mass of the end-effector) was hooked under the platform, approximately equivalent to a disturbance wrench $w_{d,1} \approx [0, 0, -50\text{N}, 0, 0, 0]^T$.
2. From 116s to 127s the platform was pulled in approximately the $\mathbf{X}_W$ direction with a wrench (measured using a mass sensor) of $w_{d,2} \approx [-100\text{N}, 0, 0, 0, 0, 0]^T$ ($\approx 384\%$ the mass of the end-effector).
3. From 143s to 155s the platform was pulled in approximately the $\mathbf{X}_W$ direction with a wrench (measured using a mass sensor) of $w_{d,3} = [100N, 0, 0, 0, 0, 0]^T$ ($\approx 384\%$ the mass of the end-effector).

With this premise in mind, we can first look at the tracking error shown in Figs. 3e and 3f. The first thing worth noting in these plots is that despite the model uncertainties the end-effector converges extremely quickly (less than half a second) to the desired trajectory, thus providing a practical proof of the finite-time convergence of the ASTC. Additionally, it is remarkable that throughout the whole experiment the tracking error remains in the same small range, even when the external disturbances are applied, confirming that the system is very robust and capable to quickly counteract even significant perturbations. Such a reactive behaviour is achieved thanks to the adaptation law (19). Indeed, the graph of the evolution of the controller gains α (Fig. 3g) reveals that in correspondence to the external disturbances the gains along the affected direction of motion increase very quickly and decrease as quickly once the disturbance is removed.

Another reason for including the adaptive gains, as explained earlier, was to reduce the effect of chattering that is common to sliding-mode controllers based on the sign() function. However, the evolution of the sliding variable σ (see Fig. 3h) shows that the chattering is still significant. The reason for this might be partially due to the fact that the parameters of the controller, in particular the saturation thresholds in the adaptation law, were not well tuned. While we do not have yet a decisive explanation to this issue, we can speculate that the dominant cause of the chattering be unmodelled dynamics of the drive train (e.g. friction, slip-stick effects, hysteresis, creeping, inhomogeneous materials, elasticity, thermal expansion and flattening of cables) or changes in the cable configuration [8] that inject vibrations in the system. For example, we think that static friction had a significant effect because we needed to apply torques much larger than expected to start moving the robot. In conclusion, this experiment suggests that further investigation is needed to quantify and understand the cause of the chattering, i.e. whether it is due to the numerical implementation of the algorithm or to the aforementioned unmodelled effects.

5 Conclusion

In this paper we presented preliminary experimental validation of a Super-Twisting sliding mode controller with adaptive gains applied to a redundant CDPR with eight cables and six degrees of freedom. The experiment showed promising characteristics of the ASTC, in terms of tracking accuracy and robustness to significant perturbations, particularly a remarkable reactivity to sudden disturbances. At the same time, the experiment also raised questions about the presence of chattering. From the preliminary results in this paper

we think that unmodelled dynamics of the power train (e.g. friction [5]) or changes in the cable configuration ([8]) might be connected to this effect, but further investigation is required. Additionally, we plan to explore possible improvements of the ASTC by combining it with interconnection-damping-assignment.

References

1. Babaghasabha, R., Khosravi, M.A., Taghirad, H.D.: Adaptive control of KNTU planar cable-driven parallel robot with uncertainties in dynamic and kinematic parameters. In: A. Pott, T. Bruckmann (eds.) Cable-Driven Parallel Robots, *Mechanisms and Machine Science*, vol. 32, pp. 145–159. Springer International Publishing (2015)
2. Cone, L.L.: Skycam-an aerial robotic camera system. Byte **10**(10), 122 (1985)
3. Duan, B., Qiu, Y., Zhang, F., Zi, B.: Analysis and experiment of the feed cable-suspended structure for super antenna. In: 2008 IEEE/ASME Int. Conf. on Advanced Intelligent Mechatronics, pp. 329–334 (2008)
4. El-Ghazaly, G., Gouttefarde, M., Creuze, V.: Adaptive terminal sliding mode control of a redundantly-actuated cable-driven parallel manipulator: CoGiRo. In: A. Pott, T. Bruckmann (eds.) Cable-Driven Parallel Robots, *Mechanisms and Machine Science*, vol. 32, pp. 179–200. Springer International Publishing (2015)
5. Kraus, W., Kessler, M., Pott, A.: Pulley friction compensation for winch-integrated cable force measurement and verification on a cable-driven parallel robot. In: Robotics and Automation (ICRA), 2015 IEEE International Conference on, pp. 1627–1632. IEEE (2015)
6. Lamaury, J., Gouttefarde, M., Chemori, A., Herve, P.E.: Dual-space adaptive control of redundantly actuated cable-driven parallel robots. In: 2013 IEEE/RSJ Int. Conf. on Intelligent Robots and Systems, pp. 4879–4886 (2013)
7. Merlet, J.P.: Solving the forward kinematics of a gough-type parallel manipulator with interval analysis. The International Journal of robotics research **23**(3), 221–235 (2004)
8. Merlet, J.P.: Checking the cable configuration of cable-driven parallel robots on a trajectory. In: Robotics and Automation (ICRA), 2014 IEEE International Conference on, pp. 1586–1591. IEEE (2014)
9. Miermeister, P., Kraus, W., Pott, A.: Differential kinematics for calibration, system investigation, and force based forward kinematics of cable-driven parallel robots. In: T. Bruckmann, A. Pott (eds.) Cable-Driven Parallel Robots, *Mechanisms and Machine Science*, vol. 12, pp. 319–333. Springer Berlin Heidelberg (2013)
10. Miermeister, P., Kraus, W., Pott, A.: Differential kinematics for calibration, system investigation, and force based forward kinematics of cable-driven parallel robots. In: A. Pott, T. Bruckmann (eds.) Cable-Driven Parallel Robots, *Mechanisms and Machine Science*, vol. 12, pp. 319–333. Springer International Publishing (2013)
11. Mikelsons, L., Bruckmann, T., Hiller, M., Schramm, D.: A real-time capable force calculation algorithm for redundant tendon-based parallel manipulators. In: 2008 IEEE Int. Conf. on Robotics and Automation, pp. 3869–3874 (2008)
12. Philipp, M., Masone, C., Heinrich, H., Joachim, T.: The cablerobot simulator - large scale motion platform based on cable robot technology. In: 2016 IEEE/RSJ Int. Conf. on Intelligent Robots and Systems (2016)
13. Pott, A.: An algorithm for real-time forward kinematics of cable-driven parallel robots. In: A. Pott (ed.) Advances in Robot Kinematics: Motion in Man and Machine, pp. 529–538. Springer International Publishing (2010)
14. Pott, A.: An algorithm for real-time forward kinematics of cable-driven parallel robots. In: Advances in Robot Kinematics: Motion in Man and Machine, pp. 529–538. Springer (2010)
15. Pott, A., Bruckmann, T., Mikelsons, L.: Closed-form force distribution for parallel wire robots. In: Computational Kinematics, pp. 25–34. Springer (2009)
16. Schenk, C., Bülthoff, H., Masone, C.: Robust adaptive sliding mode control of a redundant cable driven parallel robot. In: Int. Conf. on System Theory, Control and Computing, pp. 427–434 (2015)
17. Schenk, C., Miermeister, P., Masone, C., Bülthoff, H.: Modeling and analysis of cable vibrations on a cable-driven parallel robot. In: ICIAIEEE International Conference on Information and Automation, pp. 427–434 (2017)
18. Schmidt, V., Kraus, W., Pott, A.: Presentation of experimental results on stability of a 3 dof 4-cable-driven parallel robot without constraints. In: T. Bruckmann, A. Pott (eds.) Cable-Driven Parallel Robots, *Mechanisms and Machine Science*, vol. 12, pp. 87–99. Springer Berlin Heidelberg (2013)
19. Shtessel, Y., Edwards, C., Fridman, L., Levant, A.: Sliding Mode Control and Observation. Springer (2014)
20. Shtessel, Y.B., Taleb, M., Plestan, F.: A novel adaptive-gain supertwisting sliding mode controller: Methodology and application. Automatica **48**(5), 759–769 (2012)
21. Surdilovic, D., Bernhardt, R.: String-man: a new wire robot for gait rehabilitation. In: IEEE Int. Conf. on Robotics and Automation, pp. 2031–2036. New Orleans, Louisiana (2004)

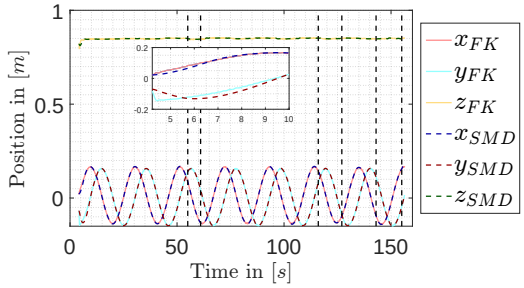

(a) Position from FK and SMD

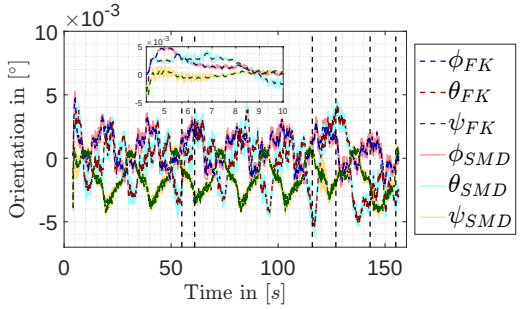

(b) Orientation from FK and SMD

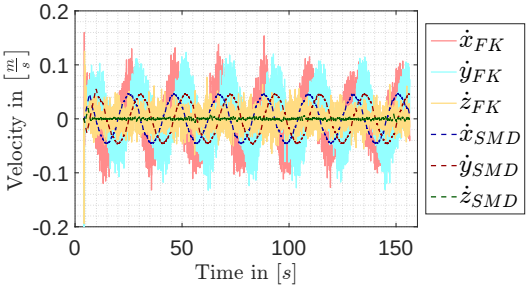

(c) Translational velocity from FK and SMD

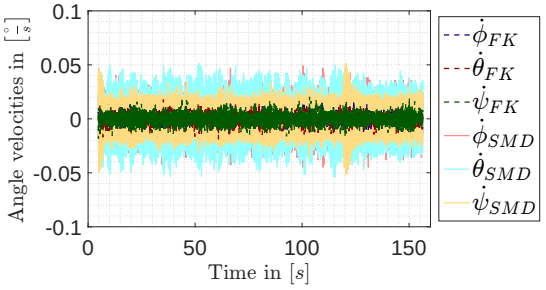

(d) Euler rates from FK and SMD

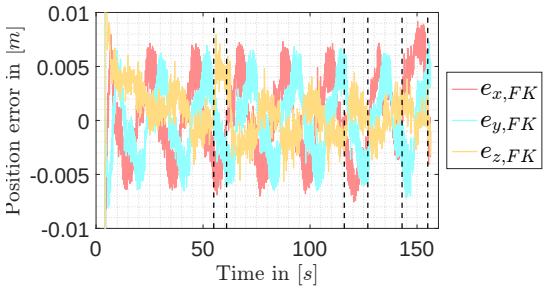

(e) Tracking Error -position-

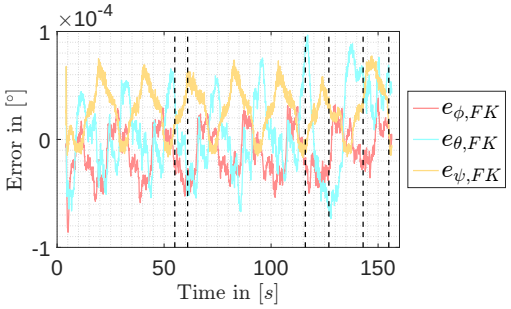

(f) Tracking Error -orientation-

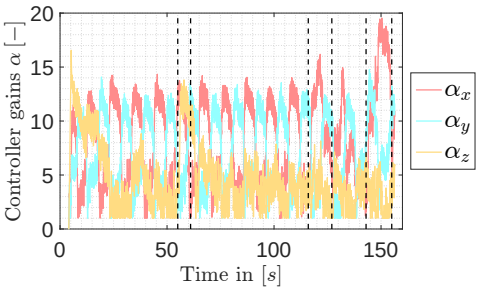

(g) Control gain α

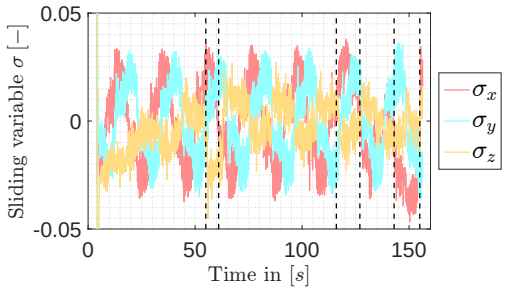

(h) Sliding variable σ

Fig. 3: Experimental results